GIGABYTES TO BYTES: AUTOMATED DENOISING AND FEATURE EXTRACTION AS APPLIED TO THE ANALYSIS OF HIV ARCHITECTURE AND VARIABILITY USING ELECTRON TOMOGRAPHY

Rajesh Narasimha[#], Adam Bennett[#], Daniel Zabransky[#], Rachid Sougrat[#], Steven McLaughlin* and Sriram Subramaniam[#]*

*[#]Laboratory of Cell Biology, Center for Cancer Research, National Cancer Institute, Bethesda, MD, *Georgia Institute of Technology, Atlanta GA,*

{rajesh,swm}@ece.gatech.edu, djzabr@wm.edu, {bennettad, sougrat}@mail.nih.gov, ss1@nih.gov

Abstract: Advances in automated data acquisition in electron tomography have led to an explosion in the amount of data that can be obtained about the spatial architecture of a variety of biologically and medically relevant objects with sizes in the "nano" range of 10-1000nm. The development of methods to analyze the vast amounts of information contained in these tomograms is a major challenge since the electron tomograms are intrinsically noisy. A fundamental step in the automatic analysis of large amounts of data for statistical inference is to segment 3D features in cellular tomograms that can work robustly and rapidly despite of low signal to noise ratios inherent to biological electron microscopy. This work evaluates various denoising techniques on tomograms obtained using dual-axis simultaneous iterative reconstruction (SIRT) technique. Using three-dimensional images of HIV in infected human macrophages as an example, we demonstrate that transform domain-denoising techniques significantly improve the fidelity of automated feature extraction. Importantly, our approaches represent an vital step in automating the efficient extraction of useful information from large datasets in biological tomography, and facilitate the overall goal of speeding up the process of reducing gigabyte-sized tomograms to byte-sized data.

Keywords: Electron tomography, Denoising, Feature extraction, HIV, Dual-Axis SIRT and Automated techniques.

1. INTRODUCTION

Electron tomography (ET) is an emerging tool to describe the three-dimensional (3D) architectures of large molecular complexes, viruses and cells. ET is a general method for three-dimensional reconstruction of electron transparent objects from a series of projection images recorded with a transmission electron microscope. At high-doses, electrons interact with unstained organic matter which leads to breaking of chemical bonds and the creation of free radicals which in turn cause further secondary damage. At low-doses it is possible to scatter of electrons from biological matter such as proteins and record molecular images, but, at the expense of poor signal-to-noise ratio (SNR) [1]. The challenge for achieving high resolution with electron imaging of unstained specimens then is that doses that are high enough to get

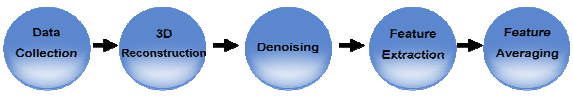

Fig. 1. Imaging Pipeline.

a good SNR lead to unacceptable specimen damage, while doses that are low enough to preserve the specimen, lead to poor image quality. Hence there is a trade-off between the dosage level and the damage caused to the specimen. The use of stains allows imaging to be carried out using higher electron doses, although this does not completely solve the problem of low SNR. The main steps in imaging and image processing are highlighted in Fig. 1.The data collection includes taking a series of images at different relative tilts of beam and specimen as shown in Fig. 2. The electron microscope provides 2D projection images. Tomograms are generated by computational analysis of a series of electron micrographs taken at varying tilt angles, usually from -80° to +80°. Using algorithms that implement weighted back projection or SIRT, one can obtain 3D volumes of the specimen from projection images as shown in Fig. 2.

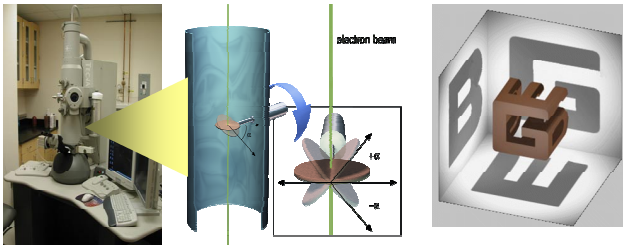

Fig. 2. Data Collection procedure (left) and reconstruction using Weighted Back Projection (WBP) (right)

As techniques for data collection and tomogram reconstruction are becoming more streamlined, the development of methods to analyze the enormous amounts of information in these tomograms remains a major challenge [1]. Efforts to establish tools for quantitative interpretation of tomograms are beginning to be applied to a range of biological problems, as reviewed recently [2]. A long-term, goal of this type of electron tomography is to interpret the spatial arrangement of the constituent molecular components at high resolution. Typically, the identification of simple structural features, such as membrane boundaries, or protein complexes, such as ribosomes, is made possible by differentially stained cellular components relative to their immediate neighbors. Electron tomograms, are, however, intrinsically noisy, and this poses significant challenges for image interpretation, especially in the context of high-throughput data collection and analysis. A fundamental step in the automatic analysis of large amounts of data for statistical inference is to employ robust methods for 3D segmentation that can work well at low SNR. The target of these strategies is to improve the signal as much as possible relative to the noise level to mine 3D information from complex tomograms.

This work investigates transform domain denoising techniques in the context of electron tomography of viruses. Image denoising approaches have been extensively investigated previously for various applications [3-7]. Our primary goal here is to evaluate the performance of a range of denoising techniques to electron tomograms recorded at room and cryogenic temperatures and study the implications of electron doses and noise on denoising of tomograms. Denoising techniques boost the SNR, facilitate better feature extraction, and enable the application of automated techniques. For analysis and feature extraction, we have used tomograms of HIV and the related virus, SIV, recorded at either

room or cryogenic temperatures, and reconstructed using SIRT-based approaches. We implemented dual-axis data collection in this work since it has less missing information in the tomogram, and we used SIRT because of the improved SNR in the reconstructed tomograms as compared to conventional back projection methods. We report here on the relative merits of a variety of denoising algorithms on the detection, clustering and the spatial distribution of spikes in SIV/HIV viruses, and have compared their performance using single-image SNR estimation and Fourier ring correlation techniques. Information on spike architecture and spacing (variability) generated from automated denoising and segmentation could be fundamental to vaccine development. The performance of these denoising methods was tested on a variety of viral and cellular tomograms and we found that the phase preserving algorithm (described in section 3) significantly improved the SNR while retaining the same overall architectural information in the tomograms. We validate our approach by comparison of semi-automated and automated segmentation procedures on tomograms recorded at both room and cryogenic temperature.

2. DATA COLLECTION AND RECONSTRUCTION TECHNIQUES

In ET, the range of tilt angles is often limited to ±80° due to the physical constraints imposed by the microscope, sample and holder which leads to a 'missing wedge' of information. This loss of information results as artifacts in the reconstruction including an elongation of the reconstruction in the direction of the optic axis, perpendicular to the tilt axis. All reconstructed volumes contain a significant level of noise that arises in part from the inherent limitations of current electron optics, such as chromatic and spherical aberration, beam incoherence, point spread, and certain terms of the lens transfer function, such as contrast transfer and inelastic scattering (although the latter can be reduced by use of an energy filter). Other sources of noise arise from the CCD detector; and in part from computational manipulation of the data, including inaccuracies in alignment of the tilt series and reconstruction of objects that have missing information in Fourier space. In the special case of cryo electron tomography the necessity of using low electron doses is an additional factor contributing to noise. The use of dual axis tomography in which two tilt series are recorded with mutually perpendicular tilt axes, reduces the missing wedge into a 'missing pyramid' [8]. We implement an algorithm based on SIRT that is performed by comparing at each iteration, re-projections of a reconstruction with each projection (image) obtained in the microscope, using the original projection series as a constraint on the output of the next iteration [9]. This procedure is known to reduce the reconstruction artifacts starting from noisy projection images.

Room temperature Tomograms: Tilt series of 90-nm-thick sections of fixed, stained, plastic-embedded HIV-infected monocyte-derived macrophages were collected through a range of ± 80°, at 2° intervals from 0° to ±50° and 1° intervals from ±50° to ±80°, on a Tecnai 12 Transmission Electron Microscope (FEI, Netherlands), at 1-µm defocus. The sample was rotated 90° and an orthogonal tilt series of the same area was collected. Prior to acquisition, both surfaces of the sections were coated with 15-nm gold fiducial markers for alignment. Images were recorded on a 4K × 4K Gatan CCD camera binned to 2K by 2K, at a magnification that produces a pixel size corresponding to 0.44 nm at the specimen level. Acquisition was automated using the Xplore3D software (FEI, Netherlands). Each tilt series was aligned using the IMOD package [10]. The aligned series were then reconstructed in either IMOD, using weighted back projection (WBP), or Inspect3D (FEI, Netherlands), using Simultaneous Iterative Reconstruction Technique (SIRT) with 17 iterations, to obtain orthogonal tomograms. The orthogonal WBP tomograms were combined in IMOD to obtain the final dual-axis WBP tomogram, and the orthogonal SIRT tomograms were combined in IMOD to obtain the final dual-axis SIRT tomogram.. By comparison, single-axis reconstructed volumes contain a relatively large missing wedge of information in Fourier space, resulting in anisotropic resolution and greater distortion of the 3-D structures of the reconstructed objects.

Cryo tomograms: We used cryo-electron tomography to analyze the three-dimensional architecture of individual SIV particles under near-native conditions. Preparations of the gp41-truncated variant of the Mac239 SIV strain were rapidly vitrified by plunge-freezing into liquid ethane cooled to ~-180°C, and imaged at 6 micron defocus at liquid nitrogen temperatures using a 300 kV electron microscope equipped with a field emission gun and an energy filter. The tilt series acquisition was done collecting an image every 3° intervals from ±65°. Since these are from unstained virus preparations, the contrast in the images arises from the intrinsic density of the virus. The spikes evident on the surface of the particles are ~ 8-10 nm wide and ~12 nm high, consistent with the dimensions expected from a trimer of gp120 molecules protruding from the surface of the virion. Projection images of the particles reveal the characteristic distribution of the putative gp120-gp41 viral spikes on the surface of the virion and a glimpse of the internal core of the virus.

3. DENOISING METHODS AND SIMULATION RESULTS

In this section we provide a brief explanation of the denoising techniques used to analyse the tomographic data. Our main goal is to apply the existing denoising techniques to both room and cryogenic temperature 3D tomograms and study their performance at various dosage levels and noise conditions. This is particularly of great interest since one denoising algorithm will not perform the best on diverse datasets. The tomograms also need to be qualitatively examined by a biological expert to determine whether the features of interest are well preserved after denoising. Thus we used both qualitative and quantitative measures to choose the optimal denoising algorithm. We implement and compare the performance of anisotropic diffusion [3] and complex diffusion algorithms [4] on electron tomograms. The equations for anisotropic diffusion in 3D are given as $I_t = \nabla.(c(x,y,z,t)\nabla I)$, where κ is the conductance parameter,

$$c(x,y,z,t) = 1/(1+\frac{|\nabla I|^2}{\kappa^2}) \text{ and } c(x,y,z,t) = e^{-\frac{|\nabla I|^2}{2\kappa^2}} \qquad (1)$$

and $I = I(x,y,z,t)$ is the 3D tomogram. For the complex diffusion,

$$I_t = \nabla.(c(\mathrm{Im}(I))\nabla I) \text{ with } c(\mathrm{Im}(I)) = e^{i\theta}/\left(1+\left(\frac{\mathrm{Im}(I)}{k\theta}\right)^2\right) \qquad (2)$$

where $\mathrm{Im}(I)$ is the imaginary value, θ is the phase angle and k is the threshold parameter. Another method of denosing is to preserve the phase data [5] by applying the continuous wavelet transform and we use log Gabor functions to construct symmetric/anti-symmetric wavelet filters. The process determines a noise threshold at each scale and shrinking the magnitudes of the filter response vectors, the phase information can be preserved

after reconstruction. The other denoising methods we used for comparison are based on translation invariant wavelets with soft thresholding [6], Bayes least-squares Gaussian scale mixtures (BLS-GSM) [7] where we used steerable pyramid wavelets and Weiner filtering. We used Wavelab and BLS-GSM MATLAB software available from the authors' website for both these methods with modifications. For all these methods we obtained the highest SNR by varying the parameters over a valid range and also making sure that the spatial features of interest are well retained.

Next, we present segmentation results on single/dual-axis and cryo tomograms facilitated by 3D denoising of tomograms. The effect of denoising is clearly evident from Fig. 3(c)&(d) and Fig. 4(a-d) where we can observe a surface with a complete membrane, distinct core, and envelope protein spikes. The quantitative analysis procedures such as peak-SNR (PSNR) and $\sqrt{MSE}$ assume that a clean image is available for analysis. For quantitative analysis of the denosing methods we implement single-image SNR estimation [11] since we are working with tomograms which are essentially stacks of 2D slices of the reconstructed volume. We compute the SNR of each slice using various denoising techniques and the result shown in Fig. 3(c) is an average SNR over 10 consecutive slices. The single-image SNR estimation method assumes that the noise is white and is uncorrelated from pixel to pixel. The SNR is given as [11]

$$SNR = \frac{\rho_{12}}{(1-\rho_{12})} = \frac{\phi_{11}^{NF}(0,0) - \mu_1^2}{\sigma_1^2 - (\phi_{11}^{NF}(0,0) - \mu_1^2)} = \frac{\phi_{11}^{NF}(0,0) - \mu_1^2}{\phi_{11}(0,0) - \phi_{11}^{NF}(0,0)} \quad (3)$$

where $\phi_{11}(0,0)$, $\phi_{11}^{NF}(0,0)$ are the autocorrelation function (ACF) of the noisy image, noise free (NF) image and ρ is the correlation coefficient. μ_1 and σ_1 are the mean and variance of the noisy image respectively. Since we do not have the noise free image, $\phi_{11}^{NF}(0,0)$ is estimated by assuming that its value is same as the ACF of the neighboring offsets as, $\left\langle \phi_{11}^{NF}(0,0) \right\rangle \approx (\phi_{11}(1,0) + \phi_{11}(0,1))/2$. This estimate is reasonable if the ACF changes slowly at the origin which is the case for room temperature and cryo tomograms. Single Image SNR estimation on a single axis/dual-axis SIRT reconstructed and cryo tomogram in Fig. 3(a) depicts that the anisotropic diffusion algorithm performs the best in terms of the SNR, but the image features are lost in the denoising process unlike the phase preserving (PP) method. For e.g., the SNR of the dual-axis SIRT noisy tomogram was boosted significantly from 8.1dB as shown in Fig. 3(a). Furthermore, we also compute the Fourier ring correlation (FRC) [12] to compare various reconstruction and denoising methods. From Fig. 3(b) we can observe that the PP method on a dual-axis SIRT reconstruction performed better than other approaches.

Segmentation procedure: Tomograms were segmented using the Amira Visualization software [13] which executes a procedure of 3D region-growing in which the largest connected area that contains the user-selected voxel and all voxels within a user-defined range of gray values is selected and can be used to generate a volume. Our threshold was based on a range relative to the seed voxel selected, although other methods using absolute scales for contrast can also be used. This procedure thus allows for "one-click" segmentation of the tomogram. Identical points in the center of each virion were selected to initiate the 3D growing process and create a surface. We also carried out semi-automated segmentation in which user-designated regions of the tomogram are subjected to a threshold (Fig. 4(a-d)). We then compare the results of the one-click segmentation for both single and dual-axis SIRT reconstructed HIV virion that was imaged at room temperature against semi-automated segmentation (second row of Fig. 4). The one-click segmentation of the denoised SA-SIRT tomogram gave a surface that resembled a virion with a core and a few envelope protein spikes (Fig. 4(f)). One-click segmentation of a non-denoised DA-SIRT tomogram returned a surface that was highly non-contiguous and included noise (Fig. 4(g)). After the tomogram was denoised, one-click segmentation yielded a surface with a complete membrane, distinct core, and envelope protein spikes that closely matched the location of the spikes from semi-automatically segmented version of the DA-SIRT denoised tomogram as in Fig. 4(h). For the single axis tomograms obtained from data recorded at cryogenic temperatures (last row, Fig. 4(i-l)) only semi-automated segmentation is possible due to the higher noise levels. The results in the denoised tomogram shown in Fig. 4(l) depict that the spikes are well separated and the spike-volume is more distinct. In Table 1, we present a comparison of the fully and semi-automated approaches on the DA-SIRT reconstructed tomogram in terms of the volume estimates of individual viral spikes. The variation between these two approaches is within 25%.

	Voxel size (Semi-Automated)	Voxel size (Automated)	Relative Error
1	942.6560	825.36	0.1244
2	757.5100	678.92	0.1037
3	962.9190	1209.40	0.2560
4	849.7470	691.77	0.1859

Table 1. Volume occupied by the viral spikes.

4. CONCLUSION AND FUTURE WORK

Electron tomograms are intrinsically noisy and this poses significant challenges for image interpretation, especially in the context of low dose and high-throughput data analysis. To maximize the information in reconstructed tomograms, we have used dual axis data collection strategies, and to obtain the highest starting SNR, we have used SIRT-based reconstruction approaches. Our goal has been to evaluate the relative performance of different denoising methods in further improving the SNR, and to test whether these denoised tomograms can be processed automatically to extract biologically relevant information. We demonstrate that denoising significantly improves the fidelity of automated feature extraction, and that phase preserving algorithm performs best for recovering structural information. We show that molecular information such as the average volume of individual viral spikes can be obtained from these denoised tomograms, and that the values closely match those obtained using manual user-guided approaches. This tool thus represents an important element in the overall pipeline for HIV imaging for analyzing the structural origins of variation in different viral isolates.

REFERENCES

[1] S. Subramaniam and J. L. S. Milne, "Three-dimensional electron microscopy at molecular resolution," *Annual Review of Biophysics and Biomolecular Structure*, pp. 141-155, 2004.

[2] A. S. Frangakis and F. Forster, "Computational exploration of structural information from cryo-electron tomograms.," *Current Opinion in Structural Biology*, vol. 14, pp. 325-331, 2004.

[3] P. Perona and J. Malik, "Scale-space and edge detection using anisotropic diffusion," *IEEE Transactions on Pattern Analysis and Machine Intelligence*, vol. 12, pp. 629--639, 1990.

[4] G. Gilboa, N. Sochen, and Y. Y. Zeevi, "Image Enhancement and Denoising by Complex Diffusion Processes," *IEEE Transactions on Pattern Analysis and Machine Intelligence (PAMI)*, vol. 26, pp. 1020-36, 2004.

[5] P. Kovesi, "Phase Preserving Denoising of Images," *The Australian Pattern Recognition Society Conference: DICTA'99*, pp. 212-217, December 1999. Perth WA.

[6] D. L. Donoho, "Denoising via soft-thresholding," *IEEE Transactions on Information Theory*, vol. 41, pp. 613-627, May 1995.

[7] J. Portilla, V. Strela, M. Wainwright, and E. P. Simoncelli, "Image Denoising using Scale Mixtures of Gaussians in the Wavelet Domain," *IEEE Transactions on Image Processing*, vol. 12, pp. 1338-1351, November 2003.

[8] P. Penczek, M. Marko, K. Buttle, and J. Frank, "Double-tilt electron tomography," *Ultramicroscopy*, vol. 60, pp. 393-410, 1995 Oct.

[9] P. Gilbert, "Iterative methods for the three-dimensional reconstruction of an object from projections," *Journal of Theoretical Biology*, vol. 36, pp. 105-17, July 1972.

[10] J. R. Kremer, D. N. Mastronarde, and J. R. McIntosh, "Computer Visualization of Three-Dimensional Image Data Using IMOD," *Journal of Structural Biology*, pp. 71-76, 1996.

[11] J. L. T. Thong, K. S. Sim, and J. C. H. Phang, "Single-Image Signal-to-Noise Ratio Estimation," *Scanning*, vol. 23, pp. 328-336, 2001.

[12] J. Frank, *Three-Dimensional Electron Microscopy of Macromolecular Assemblies: Visualization of Biological Molecules in Their Native State*: Oxford University Press, USA, 2006.

[13] "http://www.tgs.com/."

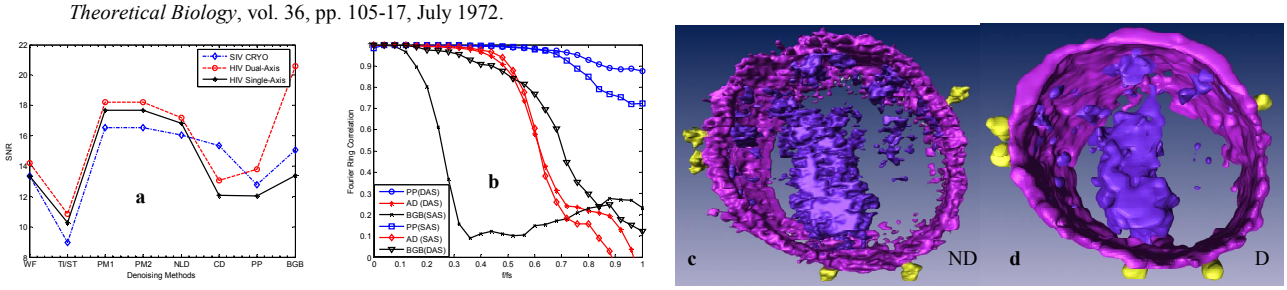

Fig. 3. (a) Single-image SNR for various denoising methods for room temperature and cryo tomograms, (WF-Weiner Filter, TI/ST-Translation invariant with soft thresholding, PM1 and PM2- Perona-Malik equations 1&2, NLD-Nonlinear Diffusion, CD-Complex Diffusion, PP-Phase preserving and BGB- BLS-GSM method. (b) Fourier Ring Correlation (FRC) for Dual-Axis and Single-Axis reconstructed HIV tomograms using various denoising methods. Semi-automted segmentation of Dual-axis SIRT reconstructed HIV tomogram (c) noisy & (d) denoised.

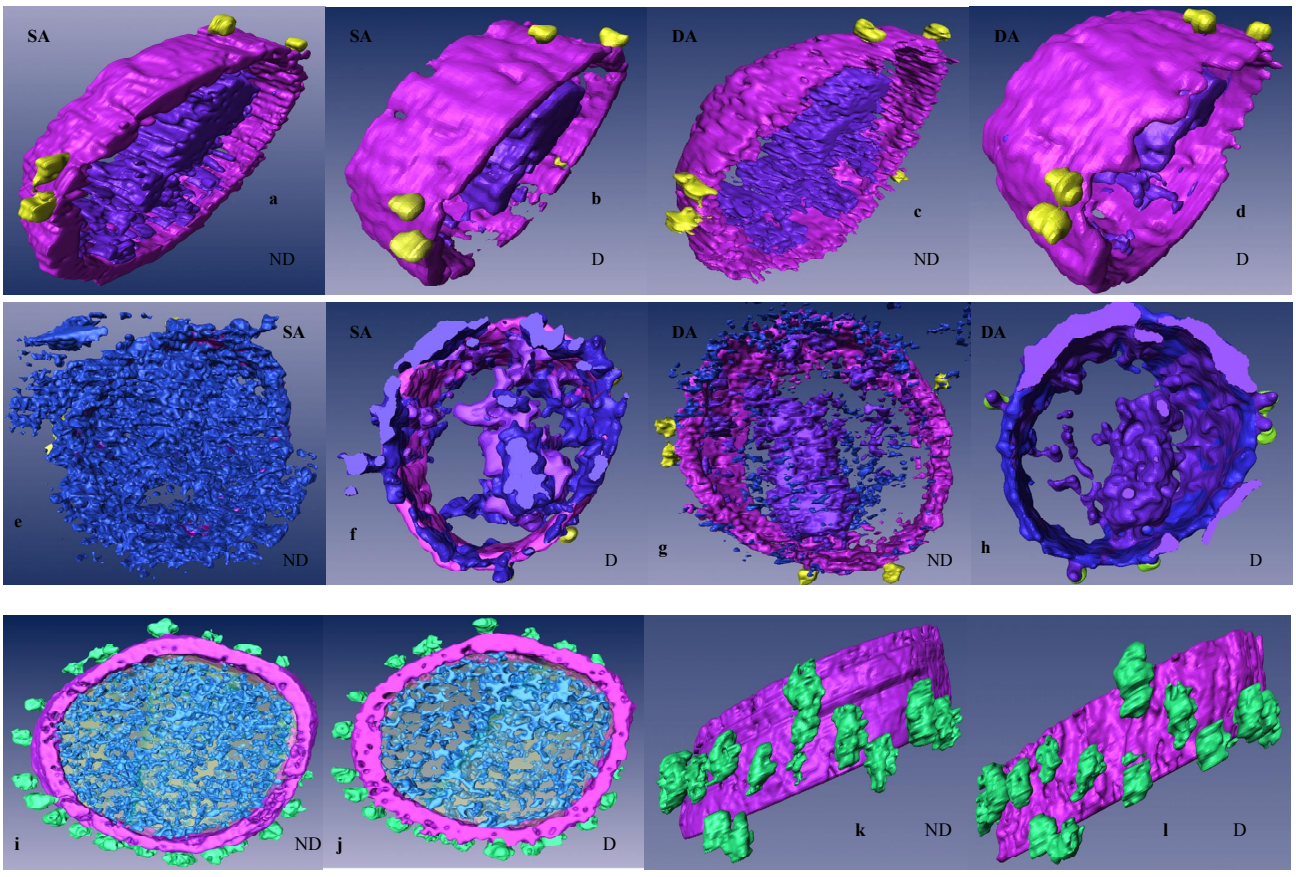

Fig. 4. Top Row (a-d): Semi-Automated Tilted. Second Row (e-h): Comparison of the Semi-Automated and Automated segmentation results. (Left two figures in each row) SA-SIRT reconstructed HIV virion & (Right two figures in each row) DA-SIRT reconstructed HIV virion. Last Row (i-l): Cryo SIV virion (Left), Cryo SIV spike spatial distribution (Right). (ND-Non Denoised, D-Denoised, SA-Single axis & DA- Dual Axis).